

Shear rheology of confined double rings of dust particles in a dusty plasma

Miao Tian(田淼), Jiaqi Li(李佳琪), Xuebo Yu(于雪波), Xue Liu(刘雪), Shaopeng Li(李绍鹏), Qing Li(李庆), Fucheng Liu(刘富成), and Yafeng He(贺亚峰)

Citation: Chin. Phys. B, 2024, 33 (**12**): 125201. DOI: 10.1088/1674-1056/ad8552
Journal homepage: http://cpb.iphy.ac.cn; http://iopscience.iop.org/cpb

What follows is a list of articles you may be interested in

Ion acoustic solitary waves in an adiabatic dusty plasma: Roles of superthermal electrons, ion loss and ionization

Qianghua Rao(饶强华), Hui Chen(陈辉), Sanqiu Liu(刘三秋), and Xiaochang Chen(陈小昌)
Chin. Phys. B, 2024, 33 (**8**): 085201. DOI: 10.1088/1674-1056/ad47e4

Differences between two methods to derive a nonlinear Schrödinger equation and their application scopes

Yu-Xi Chen(陈羽西), Heng Zhang(张恒), and Wen-Shan Duan(段文山)
Chin. Phys. B, 2024, 33 (**2**): 025203. DOI: 10.1088/1674-1056/ad082b

Quantitative simulations of ratchet potential in a dusty plasma ratchet

Shuo Wang(王硕), Ning Zhang(张宁), Shun-Xin Zhang(张顺欣), Miao Tian(田淼), Ya-Wen Cai(蔡雅文), Wei-Li Fan(范伟丽), Fu-Cheng Liu(刘富成), and Ya-Feng He(贺亚峰)
Chin. Phys. B, 2022, 31 (**6**): 065202. DOI: 10.1088/1674-1056/ac46c4

Long-time evolution of charged grains in plasma under harmonic external force and after being withdrawn

Miao Guan(管苗), Zhi-Dong Chen(陈志东), Meng-Die Li(李梦蝶), Zhong-Mao Liu(刘忠茂), You-Mei Wang(汪友梅), and Ming-Yang Yu(郁明阳)
Chin. Phys. B, 2022, 31 (**2**): 025201. DOI: 10.1088/1674-1056/ac0e27

Attenuation characteristics of obliquely incident electromagnetic wave in weakly ionized dusty plasma based on modified Bhatnagar-Gross-Krook collision model

Zhaoying Wang(王召迎), Lixin Guo(郭立新), and Jiangting Li(李江挺)
Chin. Phys. B, 2021, 30 (**4**): 045203. DOI: 10.1088/1674-1056/abe230

Shear rheology of confined double rings of dust particles in a dusty plasma

Miao Tian(田淼)[1,†], Jiaqi Li(李佳琪)[1,†], Xuebo Yu(于雪波)[1], Xue Liu(刘雪)[1], Shaopeng Li(李绍鹏)[1], Qing Li(李庆)[1], Fucheng Liu(刘富成)[1,3], and Yafeng He(贺亚峰)[1,2,3,‡]

[1] *College of Physical Science and Technology, Hebei University, Baoding* 071002, *China*
[2] *Hebei Research Center of the Basic Discipline for Computational Physics, Baoding* 071002, *China*
[3] *Hebei Key Laboratory of High-Precision Computation and Application of Quantum Field Theory, Baoding* 071002, *China*

(Received 6 August 2024; revised manuscript received 22 September 2024; accepted manuscript online 10 October 2024)

Shear rheology is a fundamental property of soft matter, which can be deformed. Although the shear rheology of fluids has been well studied at the macroscopic scale, understanding the microscopic processes of rheology at the single-particle level remains a challenging issue. Dusty plasma serves as an ideal platform for exploring microscopic dynamics of system at the individual particle level. Here, we study the shear rheology of confined double rings of strongly coupled dust particles in a dusty plasma. The outer ring is actively driven to rotate using laser illumination. Depending on the particle number, the inner ring may passively rotate following the outer ring at different angular speeds, resulting in shear rheology. The number of dust particles influences particle arrangement, which is characterized by the pair correlation function, bond-orientational order parameter, and triangle skewness. That further alters structural stability, significantly affecting the shear rheology.

Keywords: dusty plasma, soft matter, shear rheology

PACS: 52.27.Lw, 47.57.–s, 83.60.Rs **DOI:** 10.1088/1674-1056/ad8552

1. Introduction

Soft matter science deals with materials such as colloids, gels, polymers, dusty plasmas, and many biological substances that are easily deformed.[1–4] These materials share several similar physical properties, including rheology. Shear rheology focusses on the dynamic properties and flow behavior of materials and is used to study the order–disorder transition of soft materials. While the macroscopic behavior of soft matter is well understood, the microscopic processes of rheology at the single-particle level remain a significant unresolved issue. Of particular interest is the shear rheology occurring between layers of particles. Dusty plasmas and colloidal dispersions represent two ideal model systems for studying shear rheology at the individual particle level.[5]

Dusty plasma consists of charged microparticles (dust particles) immersed in a plasma.[6–12] These dust particles can acquire significant charges from the ambient plasma, typically up to 10^3–10^4 elementary charges in most experiments, resulting in the formation of a strongly coupled subsystem of dust particles. By applying a pair of oppositely-directed laser beams, the dust particles can form fully developed shear flow with a controllable shear rate by adjusting the laser power. Under different conditions, elastic deformation, defect generation, and plastic flow can also be observed.[13] As shear flow develops, melting spreads with a front moving at the transverse sound speed, and coherent longitudinal waves are excited in the flow region.[14] However, an experimental study of the shear rheology between two layers of dust particles in dusty plasma is still lacking, according to our literature search.

The shear rheology between multiple layers of colloidal particles has been experimentally observed recently.[15–19] Using a rotating holographic optical tweezers array to trap and drive colloids into active rotation, the inner layers of colloids also follow their rotation but with different angular speeds, giving rise to shear rheology. These colloidal particles do not come into physical contact with each other, typically interacting via a Yukawa pair potential similar to dust particles in plasma. The structure of the boundary layer affects the inner local hexagonal ordering.[18] The number of colloidal particles also influences the structure, local hexagonal ordering, and shear rate.

Here, we study the shear rheology between two layers of strongly-coupled dust particles in a dusty plasma by combining experiment and numerical simulation. A pair of laser beams are used to drive the outer ring of dust particles into active rotation. The stability of the dust particle arrangement depends on the particle number. When the particle number deviates from that required to form a stable hexagonal arrangement, the inner ring of dust particles begins to rotate at a different speed from the outer ring, and shear rheology is observed. The particle arrangement changes with particle number, which can be characterized by the pair correlation function, the bond-orientational order parameter, and the triangle skewness, as a result, affecting the shear rate.

[†]These authors contributed equally to this work.
[‡]Corresponding author. E-mail: heyf@hbu.edu.cn

© 2024 Chinese Physical Society and IOP Publishing Ltd

2. Experimental setup and model

Figure 1(a) illustrates the main part of our experimental setup. Two electrodes are placed horizontally and parallel within a chamber (not shown here) filled with argon gas. A transparent indium tin oxide (ITO) glass plate serves as the upper electrode, which is grounded, allowing the experimental phenomena to be observed from above using a camera. A stainless steel plate acts as the lower electrode and is connected to an radio frequency (RF, 13.56 MHz) power supply via a matching box. Uniform plasma is generated between the two electrodes via capacitively coupled discharge. Monodisperse polystyrene microspheres (dust particles) are introduced into the plasma and are suspended in-plane above the lower electrode due to the sheath electric field. These dust particles are further confined to form a condensed arrangement in the shape of two rings [Fig. 1(b)] using a glass ring on the lower electrode to prevent free expansion. To study the shear rheology, two Gaussian laser beams are directed at several dust particles on the outer ring in opposite directions, driving them to rotate with an angular speed $\bar{\omega}_o$. Meanwhile, the dust particles on the inner ring also rotate with an angular speed $\bar{\omega}_i$, as denoted in Fig. 1(b). The rotation speed depends on the laser power. For clarity, a polar coordinate system (r, θ, z) is defined as shown in Fig. 1(a).

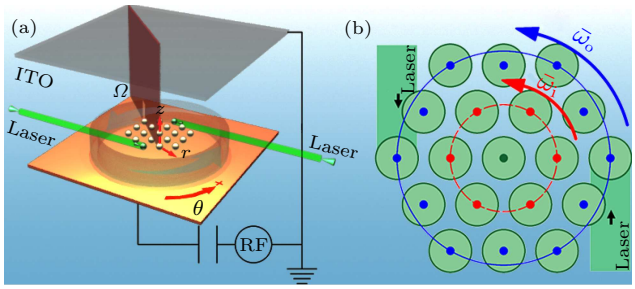


Fig. 1. Diagram of the setup: (a) uniform plasma is generated between the upper and lower electrodes. Dust particles are suspended above the lower electrode and confined by a glass ring to form a double-rings arrangement. Two laser beams illuminate several dust particles in opposite directions, driving them to rotate. (b) The dust particles on the inner and outer rings perform persistent rotation with angular speeds $\bar{\omega}_i$ and $\bar{\omega}_o$, respectively.

The experimental parameters used are: gas pressure $p =$ 10 Pa, rf power $P = 10$ W, separation between electrodes $d = 6$ cm, inner radius $r_0 = 8$ mm, outer radius $r_1 = 10$ mm, and height $h = 6$ mm of the glass ring. The power of each laser is 50 mW, with a width $l = 0.68$ mm, and the radius of the dust particle is $r_d = 7.5$ μm.

Numerical simulations are conducted based on the experimental setup model shown in Fig. 1. Due to the extensive computational requirements for three-dimensional (3D) simulation, a direct one-step simulation is currently impractical. Instead, a two-step simulation approach is used to obtain the 3D distribution of plasma parameters, leveraging the circular symmetry of the configuration.[20] Firstly, in a randomly chosen vertical cross section (r–z plane) as denoted by Ω in Fig. 1, plasma parameters $\Pi(r,z)$ are calculated via COMSOL.[21] This involves solving the continuity equations for charged species and the electron energy balance equation, coupled with Poisson's equation. Secondly, the 3D distributions of plasma parameters $\Pi(r,\theta,z)$ are obtained by rotating and interpolating the plasma parameters $\Pi(r,z)$ around the symmetric axis of the glass ring from 0 to 2π. The parameters used in the simulations match those of the experiments described above. Under these parameters, the calculated electron density $n_e = 1.78 \times 10^{15}$ m^{-3}, potential $U = 43.75$ V, and Debye length $\lambda_{De} = 457$ μm. The potential within the glass ring shows a parabolic distribution, which confines the negatively charged dust particles to the center of the glass ring to form an approximate two-dimensional (2D) arrangement.

Based on the calculated plasma parameters, the charge Q of a dust particle can be obtained using OML theory, which yields $Q \sim 10^4 e$. The forces acting on the dust particles can then be analyzed, and the equation of motion for a dust particle can be described as follows:[22,23]

$$m\ddot{\boldsymbol{r}} = \boldsymbol{F}_g + \boldsymbol{F}_i + \boldsymbol{F}_n + \boldsymbol{F}_Y + \boldsymbol{F}_e + \boldsymbol{F}_L + \boldsymbol{F}_\eta, \tag{1}$$

here, m represents the mass of the dust particle, $\ddot{\boldsymbol{r}}$ is the acceleration of the dust particle. The forces acting on the dust particle include the gravity force $\boldsymbol{F}_g$, the ion drag force $\boldsymbol{F}_i$,[8] the neutral drag force $\boldsymbol{F}_n$,[6] the interparticle force $\boldsymbol{F}_Y$,[24] the electric force $\boldsymbol{F}_e$, the laser propulsion force $\boldsymbol{F}_L$,[25] and the fluctuation force $\boldsymbol{F}_\eta$.

The laser propulsion force is related to the intensity of the applied laser beam:

$$F_L = q\big((n\pi r_d^2 I_L)/c\big), \tag{2}$$

where q is a dimensionless factor determining the absorptivity of photons, which is assumed to be unity, representing full absorption; $n = 1$ is the refractive index of the surrounding media, and c is the speed of light. Under the present experimental conditions, $F_L \sim 10^{-12}$ N.

3. Results

Under the present experimental conditions, the subsystem of dust particles exhibits a strongly coupled feature, resulting in a relatively stable configuration that depends on the particle number. For the particle numbers $N = 18$, 19, and 20 used here, the effective area fraction $\phi_{eff} \sim 0.8$–0.9, suggesting a hexagonal configuration.[18] When the number of introduced dust particles is $N = 19$, as shown in Fig. 2, they form a static configuration with hexagonal symmetry in the absence of laser illumination. This configuration consists of a central core with 1 particle, an inner ring with 6 particles, and an outer ring with 12 particles, arranged as (1, 6, 12) for the magic number of 19. For convenience, these dust particles are labelled as a core (1), an inner ring (2–7), and an outer ring (8–19), as indicated in

Fig. 2. When the lasers are turned on, the two laser beams illuminate four dust particles on the outer ring at fixed positions (17, 18, 11, and 12) in Fig. 2(a) in opposite directions. These four dust particles push their neighboring dust particles on the same outer ring, generating persistent rotation in an anticlockwise direction. This behavior is shown in Figs. 2(a)–2(c) for experimental observations and Figs. 2(d)–2(f) for simulations. The period of the actively rotating outer ring is approximately $T \sim 30.1$ s, observed experimentally with a laser power of 50 mW. Increasing the laser power definitely enhances the laser propulsion force, as a result, accelerating the rotation speed of the particles. In addition, the height difference of the suspended particles is only at the micrometer-scale. Compared with the millimeter-scale structure formed by dust particles in the r–θ plane, the distribution of dust particles in the z direction can be neglected.

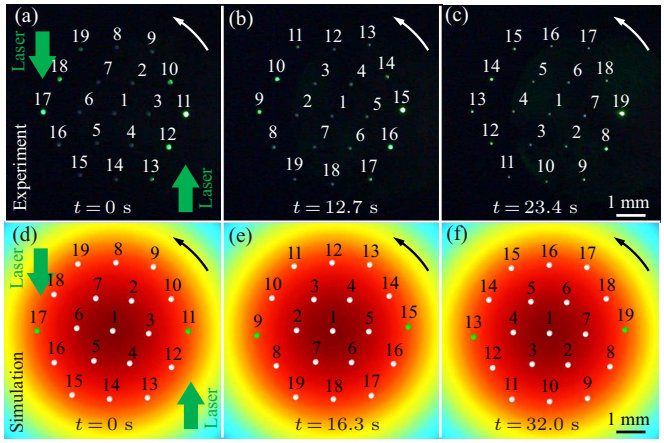


Fig. 2. Spatial distributions of dust particles with a number of $N = 19$ [arranged as (1, 6, 12)] and their rotation process in an anticlockwise direction. Laser beams illuminate the dust particles at fixed positions, as denoted by 17, 18, 11, and 12 in panel (a), in opposite directions. (a)–(c) Experiment, (d)–(f) simulation. The inner ring rotates with the same angular speed as the outer ring. Gas pressure $p = 10$ Pa, rf power $P = 10$ W, and laser power $P_{\rm laser} = 50$ mW.

The dust particles on the inner ring passively rotate as a rigid body at the same speed as those on the outer ring, which is attributed to the strong coupling among them and the stable configuration for the magic number of $N = 19$. The curve of angular displacement versus time for a randomly selected dust particle on the inner ring closely matches that of a dust particle on the outer ring, as shown in Fig. 3. This indicates rigid rotation for this configuration, with the rotation speed $\bar{\omega}_{\rm i} = \bar{\omega}_{\rm o} = 0.209$ rad/s in experiment and $\bar{\omega}_{\rm i} = \bar{\omega}_{\rm o} = 0.131$ rad/s in simulation.

When the number of introduced dust particles deviates from $N = 19$, which is the magic number required for a stable configuration, the dynamical processes change markedly. For example, when $N = 18$, the subsystem of dust particles forms a configuration with the arrangement (1, 6, 11), as shown in Fig. 4(a). In this case, under laser illumination, both the inner and outer rings rotate persistently but at different speeds [see Figs. 5(a) and 5(c)], with $\bar{\omega}_{\rm i} < \bar{\omega}_{\rm o}$, indicating that the inner ring rotates slower than the outer ring, suggesting a slip between the two rings. The calculated shear rate, which characterizes the shear rheology, is $\gamma = r_{\rm i}\Delta\bar{\omega}_{\rm o,i}/\Delta r_{\rm o,i} = 0.69$ s^{-1} for this configuration, where $\Delta\bar{\omega}_{\rm o,i} = \bar{\omega}_{\rm o} - \bar{\omega}_{\rm i}$ is step down in $\bar{\omega}$ between the outer and inner rings, and $\Delta\bar{r}_{\rm o,i} = \bar{r}_{\rm o} - \bar{r}_{\rm i}$ is the radial separation between the rings.[17] During the slipping process, the inner ring maintains its hexagonal symmetry, as shown in Figs. 4(a)–4(c). Therefore, the observed slipping results from the reduction in symmetry of the outer ring, which leads to decrease in structural stability. Furthermore, the shear rheological behavior is explicitly correlated with the applied shear rate. This phenomenon is very similar to what has been observed in colloidal experiments.[19]

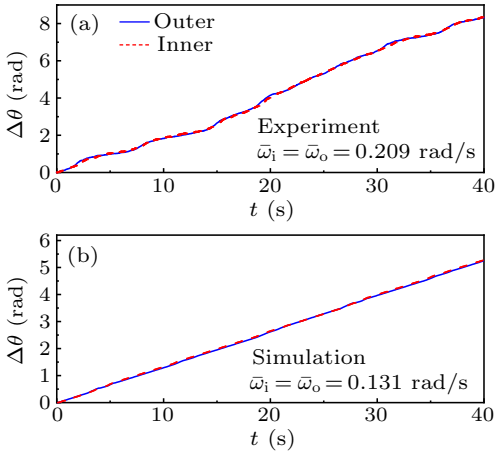


Fig. 3. Dependence of the angular displacements of two randomly-selected rotating dust particles on the inner and outer rings over time: (a) experiment, (b) simulation. The dashed curve and the solid curve coincide with each other, suggesting identical rotation speeds, $\bar{\omega}_{\rm i} = \bar{\omega}_{\rm o}$, on the inner and outer rings. The parameters used are the same as those in Fig. 2. The two randomly-selected rotating dust particles are No. 7 and No. 17 as indicated in Fig. 2.

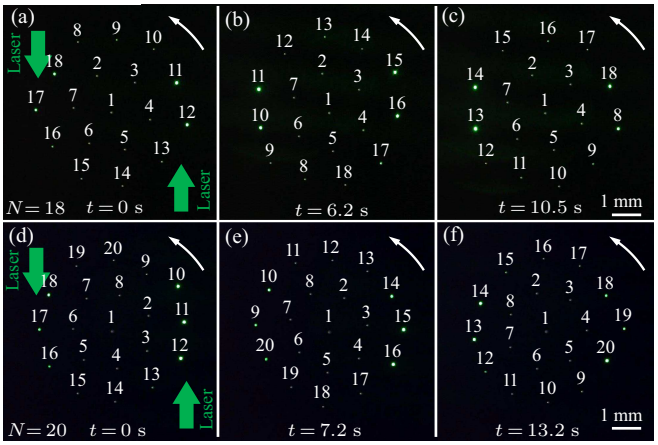


Fig. 4. Spatial distributions of dust particles and their rotation process: (a)–(c) $N = 18$, arranged as (1, 6, 11); (d)–(f) $N = 20$, arranged as (1, 7, 12). The outer ring rotates faster than the inner ring. Gas pressure $p = 10$ Pa, rf power $P = 10$ W, and laser power $P_{\rm laser} = 50$ mW.

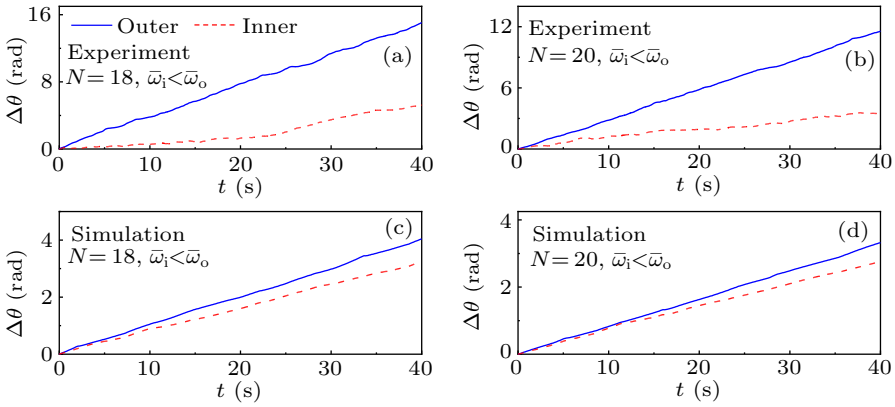


Fig. 5. Dependence of the angular displacements of two randomly-selected rotating dust particles on the inner and outer rings over time: (a)–(b) experiments for $N = 18$ and 20, (c)–(d) simulations for $N = 18$ and 20, respectively. The dashed curve deviates from the solid curve, suggesting different rotation speeds, $\bar{\omega}_i < \bar{\omega}_o$, on the inner and outer rings. The parameters used are the same as those in Fig. 4. The two randomly-selected rotating dust particles are No. 7 and No. 17 as indicated in Fig. 4.

For the case of $N = 20$, the subsystem of dust particles forms a configuration with the arrangement (1, 7, 12), as shown in Fig. 4(d). Under laser illumination, the inner ring also begins to rotate passively, following the active outer ring [Figs. 4(d)–4(f)], but at a slower angular speed, $\bar{\omega}_i < \bar{\omega}_o$, as shown in Figs. 5(b) and 5(d). The seven particles on the rotating inner ring result in decrease of structural stability, leading to similar shear behavior between the inner and outer rings, with a shear rate $\gamma = 0.52$ s^{-1}. It is noteworthy that the reversal of the laser direction does not exert influences on the results beyond the rotation direction. Furthermore, the shear rheological behavior is explicitly correlated with the applied shear rate. If the laser power is below 10 mW, shear rheology disappears even under the conditions of $N = 18$ and $N = 20$. However, increasing the laser power to a level of 100 mW as we test still does not lead to the shear rheology even for $N = 19$.

To quantify the influence of structural stability on shear rheology, we present the tangential stress on the inner ring σ_i based on the following formula:[16]

$$\sigma_i = \frac{\zeta n_i \bar{r}_i \omega_i}{\pi(r_i + r_o)}, \tag{3}$$

here, ζ represents the drag coefficient according to the Epstein formula, and n_i represents the particle number of the inner ring. Both results in experiment and simulation indicate that the shear stress between the inner and outer rings σ_i is greater when the number of particles $N = 19$ compared to cases where $N = 18$ or $N = 20$, which directly accounts for the occurrence of shear rheology under conditions of $N = 18$ and $N = 20$ particles.[20] Here, we provide the specific magnitude of σ_i. When $N = 18$, 19, and 20, $\sigma_i = 6.17 \times 10^{-10}$ N/m, 9.85×10^{-10} N/m, and 4.84×10^{-10} N/m in experiment, respectively, and $\sigma_i = 3.83 \times 10^{-10}$ N/m, 6.17×10^{-10} N/m, and 3.82×10^{-10} N/m in simulation, respectively.

The observed shear rheology originates from changes in the structure of the dust particles. For the stable structure with $N = 19$, the pair correlation function g_r exhibits distinct narrow peaks, as indicated in Figs. 6(b) and 6(e). This structure displays a better hexagonal symmetry, which can be evaluated using the triangle skewness[26] defined by

$$S = \max[(\phi_{max} - \phi_e)/(\pi - \phi_e), (\phi_e - \phi_{min})/\phi_e], \tag{4}$$

here, ϕ_{max} and ϕ_{min} represent the largest and smallest angles in the triangle faces, as shown in Fig. 7, $\phi_e = \pi/3$ for triangle, $S = 0$ for perfect hexagonal symmetry, and the hexagonal symmetry decreases as S increases.

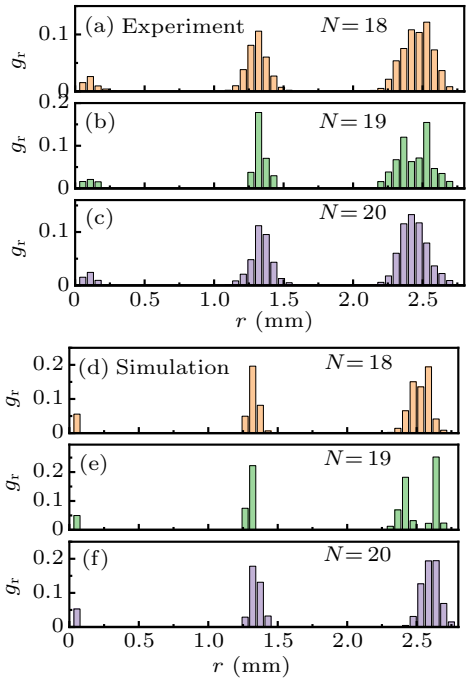


Fig. 6. Pair correlation function g_r for different particle numbers N: (a)–(c) experiment, (d)–(f) simulation. The parameters are the same as those in Fig. 4.

In Figs. 7(b) and 7(e), for $N = 19$, the triangle skewness approaches zero, suggesting a hexagonal arrangement. This is further verified by the bond-orientational order parameter Φ_6 approaching unity as shown by the black solid curves in Fig. 8.

For the particle numbers $N = 18$ and 20, the pair correlation function g_r exhibits broad peaks, indicating decrease in structural stability of both the inner and outer ring. The symmetry of the structure also decreases as indicated by the increased triangle skewness shown in Figs. 7(a), 7(c), 7(d), and 7(f), particularly those between the inner and outer rings.

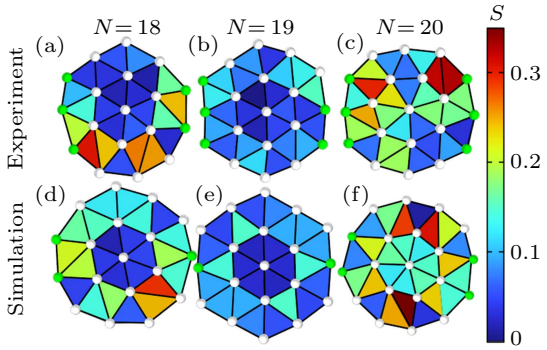


Fig. 7. Triangle skewness for different particle numbers N: (a)–(c) experiment, (d)–(f) simulation. Parameters are the same as those in Fig. 4.

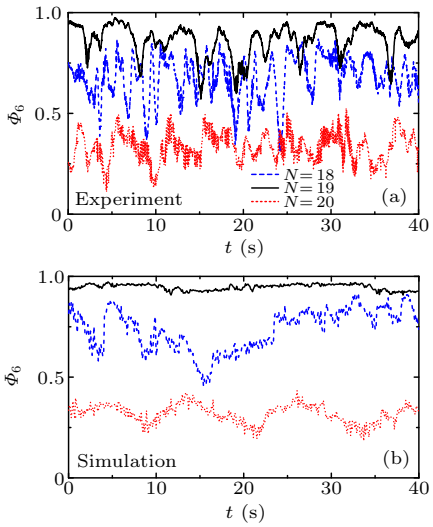


Fig. 8. Evolution of the bond-orientational order parameter for different particle numbers N: (a) experiment, (b) simulation. Parameters are the same as those in Fig. 4.

The bond-orientational order parameters Φ_6 for $N = 18$ and 20 are somewhat lower than those for $N = 19$, as shown in Fig. 8. In particular, for $N = 20$, the average value of Φ_6 is only approximately 0.3, due to the structural stability of the inner ring. The evolution of the bond-orientational order parameters with time exhibits some oscillation, which is attributed to the intermittent illumination from the laser beam on the rotating dust particles.

The structural stability is also related to the average potential energy W of the particles, which is expressed as following formula:

$$W = W_s + W_E. \tag{5}$$

In the above equation, W_s represents the parabolic potential energy of the multi-particle system, and W_E represents the interaction potential energy of the multi-particle system. The parabolic potential energy W_{s1} is determined by formulas as follows:

$$W_{s1}(x_s(t_k)) = W_{s0} - \frac{m}{2}\dot{x}_s^2(t_k) - R\int_{t_0}^{t_k} \dot{x}_s^2(\tau)\,\mathrm{d}\tau, \tag{6}$$

where W_{s0} is a constant, $x_s(t)$ and $\dot{x}_s(t)$ are the measurable trajectory of a freely released particle and its derived velocity, respectively. The relaxation time τ is determined by a linearity constant R and the particle mass m. Detailed solution methods can be found in Ref. [26]. As for parabolic potential energy W_s can be determined by the following equation:

$$W_s = \frac{1}{N}\sum_{k=1}^{N} W_{s1}(|\boldsymbol{r}_k - \boldsymbol{r}_1|), \tag{7}$$

here, $\boldsymbol{r}_k$ denotes position vector of the No. k particle ($k = 1, 2, \ldots, N$), $\boldsymbol{r}_1$ denotes position vector of the central particle. The determination of interaction potential energy W_E is governed by the subsequent formulas:

$$W_E = \frac{1}{N}\sum_{j\neq k}^{N} \frac{Kq_kq_j}{|\boldsymbol{r}_k - \boldsymbol{r}_j|}\exp\left(-\frac{|\boldsymbol{r}_k - \boldsymbol{r}_j|}{\lambda_D}\right). \tag{8}$$

In the aforementioned formula, K represents electrostatic force constant, λ_D represents the Debye length, $\boldsymbol{r}_j$ represents position vector of the No. j particle, q_k and q_j denote the charge of the No. k particle and the No. j particle ($k, j = 1, 2, \ldots, N$), respectively. In the absence of driving laser, the experiment reveals that the average potential energy of the particles reaches its minimum $W = 2.22 \times 10^{-2}$ J when the number of particles N is 19. And, its minimum is $W = 1.31 \times 10^{-2}$ J in simulation. As N gradually deviates from 19, the structure stability decreases, and the average potential energy of the particles gradually increases.[20]

4. Conclusion

By combining experiments and numerical simulations, we studied the shear rheology between two layers of strongly coupled dust particles in a dusty plasma. The outer ring is actively driven by laser illumination. Shear rheology is observed by varying the number of introduced particles. During this process, the inner ring also rotates, following the outer ring but at different angular speeds. The number of particles can affect particle arrangement, further altering the shear rate by changing structural stability. The observed shear rheology in this dusty plasma system is similar to that in recent colloidal experiments. Both systems serve as ideal platforms for studying the fundamental properties of adaptive confinement in 2D materials. Future experiments with a larger number of particles could lead to the formation of multiple rings of strongly coupled dust particles, enabling accurate measurements of osmotic pressure, transverse shear rate, and longitudinal shear rate.

Acknowledgements

Project supported by the National Natural Science Foundation of China (Grant Nos. 12275064 and 12475203), the Natural Science Foundation of Hebei Province, China (Grant No. A2024201020), the Regional Key Projects of the National Natural Science Foundation of China (Grant No. U23A20678), the Scientific Research and Innovation Team Project of Hebei University (Grant No. IT2023B03), and the Post-graduate's Innovation Fund Project of Hebei University (Grant No. HBU2024BS007).

References

[1] Chaudhuri M, Ivlev A V, Khrapak S A, Thomas H M and Morfill G E 2011 *Soft Matter* **7** 1287
[2] Truby R L and Lewis J A 2016 *Nature* **540** 371
[3] Lu X and Keidar M 2019 *Mat. Sci. Eng. R.* **138** 36
[4] Ivlev A V, Löwen H, Morfill G E and Royall C P 2012 *Complex Plasmas and Colloidal Dispersions: Particle-resolved Studies of Classical Liquids and Solids* (Singapore: World Scientific Publishing Co. Pte. Ltd.) p. 9
[5] Morfill G E and Ivlev A V 2009 *Rev. Mod. Phys.* **81** 1353
[6] Du C R, Nosenko V, Thomas H M, Lin Y F, Morfill G E and Ivlev A V 2019 *Phys. Rev. Lett.* **123** 185002
[7] He Y F, Ai B Q, Dai C X, Song C, Wang R Q, Sun W T, Liu F C and Feng Y 2020 *Phys. Rev. Lett.* **124** 075001
[8] Guan M, Chen Z D, Li M D, Liu Z M, Wang Y M and Yu M Y 2022 *Chin. Phys. B* **31** 025201
[9] Qi X H, Duan W S, Chen J M and Wang S J 2011 *Chin. Phys. B* **20** 025203
[10] Yuan C X, Yao J F, Bogdanov D V, Bogdanov E A, Kudryavtsev A A and Zhou Z X 2019 *Plasma Sources Sci. Technol.* **28** 095020
[11] Zhang R Y, Liu Y H, Huang F, Chen Z Y and Li C Y 2017 *Chin. Phys. Lett.* **34** 075203
[12] Nosenko V and Goree J 2004 *Phys. Rev. Lett.* **93** 155004
[13] Feng Y, Goree J and Liu B 2010 *Phys. Rev. Lett.* **104** 165003
[14] Williams I, Oğuz E C, Jack R L, Bartlett P, Löwen H and Royall C P 2014 *J. Chem. Phys.* **140** 104907
[15] Williams I, Oğuz E C, Löwen H, Poon W C K and Royall C P 2022 *J. Chem. Phys.* **156** 184902
[16] Williams I, Oğuz E C, Speck T, Bartlett P, Löwen H and Royall C P 2016 *Nat. Phys.* **12** 98
[17] Williams I, Oğuz E C, Bartlett P, Löwen H and Royall C P 2013 *Nat. Commun.* **4** 2555
[18] Gerlof S, Ortiz-Ambriz A, Tierno P and Klapp S H L 2020 *Soft Matter* **16** 9423
[19] See supplemental material for "shear rheology of confined double rings of dust particles in a dusty plasma"
[20] COMSOL Multiphysics v. 5.3a. cn.comsol.com. COMSOL AB, Stockholm, Sweden
[21] Tian M, Yao T Y, Cai Z M, Liu F C and He Y F 2024 *Acta Phys. Sin.* **71** 115201 (in Chinese)
[22] Wang S, Zhang N, Zhang S X, Tian M, Cai Y W, Fan W L, Liu F C and He Y F 2022 *Chin. Phys. B* **31** 065202
[23] Wang K, Huang D and Feng Y 2019 *Phys. Rev. E* **99** 063206
[24] Liu B, Goree J, Nosenko V and Boufendi L 2003 *Phys. Plasmas* **10** 9
[25] Pendenza A, Habashi W G and Fossati M 2015 *Int. J. Numer. Meth. Fluids* **79** 215
[26] Konopka U and Morfill G E 2000 *Phys. Rev. Lett.* **84** 891